

First principle study of intrinsic defects in hexagonal tungsten carbide

Xiang-Shan Kong^a, Yu-Wei You^a, J. H. Xia^a, C. S. Liu^{a,*}, Q. F. Fang^a,
G.-N. Luo^b, Qun-Ying Huang^b

^a*Key Laboratory of Materials Physics, Institute of Solid State Physics, Chinese Academy of Sciences, P. O. Box 1129, Hefei 230031, P. R. China;*

^b*Institute of Plasma Physics, Chinese Academy of Sciences, Hefei 230031, P. R. China*

Abstract

The characteristics of intrinsic defects are important for the understanding of self-diffusion processes, mechanical strength, brittleness, and plasticity of tungsten carbide, which present in the divertor of fusion reactors. Here, we use first-principles calculations to investigate the stability of point defects and their complexes in WC. Our calculation results confirm that the formation energies of carbon defects are much lower than that of tungsten defects. The outward relaxations around vacancy are found. Both interstitial carbon and interstitial tungsten atom prefer to occupy the carbon basal plane projection of octahedral interstitial site. The results of isolated carbon defect diffusion show that the carbon vacancy stay for a wide range of temperature because of extremely high diffusion barriers, while carbon interstitial migration is activated at lower temperatures for its considerable lower activation energy. These results provide evidence for the presumption that the 800K stage is attributed by the annealing out of carbon vacancies by long-range migration.

⁰*Author to whom correspondence should be addressed. Email address: cslu@issp.ac.cn Tel: 0086-551-5591062

Keywords: Tungsten carbides, density function theory, intrinsic defect, diffusion

1. Introduction

The International Thermonuclear Experimental Reactor (ITER) is designed with a beryllium first wall, tungsten armor in the baffle and divertor regions, and carbon strike point plates [1, 2, 3]. Due to high particle and heat loads, the wall material will be eroded and migrate as plasma impurity to other parts. This leads to the formation of mixed material layers on the wall surface. Previous studies have indicated that a tungsten carbide layer could be formed during the bombardment of tungsten by carbon impurity [4, 5, 6]. In addition, WC is of practical interest for engineering application due to its high melting points, extreme hardness, good corrosion and temperature stability [7, 8, 9].

Tungsten carbide is stable in a hexagonal structure, which consists of alternating simple hexagonal layers of carbon and layers of tungsten. Extensive theoretical studies have been performed to understand the electronic structure and the origin of properties of hexagonal tungsten carbide such as hardness, bulk module and stability [10, 11, 12, 13]. While, much less information is available for the intrinsic defects of hexagonal tungsten carbide, which are important for the understanding of self-diffusion processes, mechanical strength, brittleness, and plasticity. This may be related to the relatively low concentration of atomic defects on the metal and the carbon sublattices. However, the defect concentration would increase greatly in tungsten carbide upon high-energy irradiation.

Remple *et al.* [14] firstly identified carbon and tungsten vacancies by positron annihilation method and found the former to be formed preferentially. Then, Ivanovskii *et al.* [15, 16] studied the effect of tungsten and carbon vacancies on the tungsten carbide band structure using first-principles full-potential linear muffin-tin orbital approach. A vacancy peak of the DOS was observed and the formation energies of defects were calculated, i.e. 0.13 Ry (1.77 eV) and 0.20 Ry (2.72 eV) for carbon and tungsten vacancy, respectively. Thereafter, Juslin *et al.* [17] and Björkas *et al.* [18] employed the molecular dynamic method to investigate the intrinsic defects in hexagonal tungsten carbide. They also gave the formation energy of tungsten/carbon vacancy and interstitial: about 12 eV for tungsten interstitial and 3 eV for tungsten vacancy; 2.7 and 0.5 eV for carbon interstitial and vacancy, respectively. Comparing with the results of Ivanovskii [15], the difference between carbon and tungsten defect formation energies is considerably large. Recently, Björkas *et al.* [18] studied the initial state of irradiation damage in tungsten carbides using molecular dynamics computer simulations. They found that irradiation of tungsten carbide induce major elemental asymmetries in defect production. This effect was explained by the large difference between tungsten and carbon defect formation energy. Even though certain details of the electronic structure and formation energy of intrinsic defects in hexagonal tungsten carbide have been addressed by aforementioned studies, several questions on the structure and stability of native point defects of tungsten carbide remain open, including questions about the atomic-scale mechanisms of defect migration.

In this paper we employ first-principles calculations to study the six possi-

ble types of native point defects of hexagonal tungsten carbide: carbon (V_C) and tungsten (V_W) vacancies, carbon (C_W) and tungsten (W_C) antisites, and carbon (I_C) and (I_W) tungsten interstitials. The formation energies of point defects are obtained, and the most stable interstitial configurations are identified by relaxing various possible configurations of carbon and tungsten interstitial structure. Besides, we investigate the atomic-scale mechanisms of isolated carbon defect migration by the nudged elastic band method. Our calculations will provide a useful reference for further exploration of the defect properties in tungsten carbide.

2. Computation method

The present calculations have been performed within density functional theory as implemented in the Vienna *ab initio* simulation package (VASP) [19, 20]. The interaction between ions and electrons is described by the projector augmented wave potential (PAW) method [21, 22]. Exchange and correlation functions are taken in a form proposed by Perdew and Wang (PW91) [23] within the generalized gradient approximation (GGA). The supercell approach with periodic boundary conditions is used to study defect properties, as well as defect free system. The perfect supercell contains 128 atoms (64 carbon atoms and 64 tungsten atoms) with $4 \times 4 \times 4$ unit cells. The relaxations of atomic position and optimizations of the shape and size of the supercell are performed with the plane-wave basis sets with the energy cutoff of 500 eV throughout this work, which was checked for convergence to be within 0.001 eV per atom in the perfect supercell. Ion relaxations are performed using the standard conjugated-gradient algorithms as implemented in

the VASP code. During the relaxations, the Brillouin zone (BZ) integrations is achieved using a Methfessel-Pazton smearing of $\sigma=0.39$ eV. BZ sampling was performed using the Monkhorst-Pack scheme [24], with a $3 \times 3 \times 3$ k -point mesh centered on the Gamma point. The structural optimization is truncated when the forces converge to less than 0.01eV.

The ground-state properties of hexagonal tungsten carbide, including equilibrium lattice parameters and bulk cohesive energy, have been calculated in order to compare with experimental and former theoretical data. Results are presented in Table 1. In addition, we obtained the bulk modulus by fitting the volume and calculated cohesive energy to Murnaghan's equation of the state. It can be seen from Table 1 that our results are in agreement with the experimental and former theoretical values.

The formation energy of intrinsic defect is given by

$$E_f = E - \frac{1}{2}(n_w + n_c)\mu_{wc} - \frac{1}{2}(n_w - n_c)(\mu_w - \mu_c), \quad (1)$$

where E is the cohesive energy of supercell with intrinsic defect, n_w and n_c are the numbers of tungsten and carbon in supercell, and μ_{wc} , μ_w and μ_c are the chemical potential of tungsten carbide, tungsten and carbon, respectively. Here, μ_{wc} is taken as the cohesive energy (per formula) of hexagonal tungsten carbide, while μ_w and μ_c are the cohesive energy (per atom) of metallic *bcc*-W (per atom) and graphite (per atom) at their optimized geometries, respectively.

3. Results and discussion

3.1. Electronic properties

Firstly, we investigate the electronic properties of perfect tungsten carbide. The density of states (DOS) and valence charge density of hexagonal tungsten carbide are shown in Fig. 1 and Fig. 2. The DOS are calculated for $3 \times 3 \times 3$ supercells. $13 \times 13 \times 13$ k -grids mesh centered on the Gamma point were obtained for Brillouin zone integrations with tetrahedron method. For the total DOS, we can see that the Fermi level (EF) is situated close to a minimum of the DOS that qualitatively indicates the stability of this material. The similarity in the shapes of the tungsten d -projected DOS and the carbon p -projected DOS reflects that strong hybridization occurs between the tungsten d and carbon p states. These results are consistent with previous theoretical studies [11, 13, 28].

3.2. Vacancies and antisite defects

There are two types of vacancies in the hexagonal tungsten carbide, namely tungsten and carbon vacancy. For the carbon vacancy, there are six equivalent tungsten atoms as its nearest-neighbors ($W_{V_c}^N$). The nearest-neighbor distance is 2.214 Å. Moreover, there are also distinct neighbor sites of carbon vacancy aligned along the c axis and in the basal plane in carbon sublattice, denoted by $C_{V_c}^c$ and $C_{V_c}^b$, respectively. Their distances away from the vacancy site are very close, 2.854 and 2.932 Å, respectively. Similar neighbors exist for tungsten vacancy, and marked with $C_{V_w}^N$, $W_{V_c}^c$ and $W_{V_c}^b$. Besides, there exist two types of antisite defects that are formed by atoms located on the wrong sublattices, namely C_W and W_C , with a carbon atom

on a tungsten site and a tungsten atom on carbon site, respectively. These initial defect configurations are relaxed using the DFT method described above, and the formation energy can be obtained from the total energy of the supercell with and without defects using Eq. (1). In addition, the defect volume changes relative to perfect tungsten carbide are calculated by

$$\Delta V/V = \frac{V_{defect} - V_0}{V_0}, \quad (2)$$

where V_{defect} and V_0 are the volume of supercell with and without defect, respectively. All calculated results are summarized in Table 2 and 3.

For the vacancy defects, we find that the nearest-neighbor atoms of the vacancy relax outward, while other neighbors move inward. It is this cooperative relaxation that makes the supercell volume insensitive to the presence of vacancies at small vacancy concentration. The volume relaxations are generally small, and the defect volume changes relative to the perfect system are -0.2% and -0.4% for V_C and V_W , respectively. Similar relaxation features have been found in other transition-metal carbide, such as titanium carbide [29]. The formation energy of V_C and V_W are 0.39 eV and 4.14 eV, respectively, and the later is much larger than the former. This is generally consistent with previous molecular dynamic calculations[17, 18], but contrasts to Ivanovskii’s results [15]. This large difference may arise from the difference in electronic properties between tungsten and carbon in hexagonal tungsten carbide. In the perfect tungsten carbide, tungsten and carbon atoms have [WC6W8] and [CW6] coordination polyhedra, respectively. It needs six W-C bonds breaking to form a carbon vacancy, whereas, eight W-W bonds also need to be broken to form a tungsten vacancy. Therefore, more energy will be needed for the tungsten vacancy formation. For the antisite

defects, the formation energy of C_W and W_C are significantly larger than that of vacancy, 8.81 and 8.69 eV, respectively. This indicates that antisites are energetically less favorable. The outward relaxation around W_C is considerably large, and the defect volume change is 3.4%. It should be pointed out that the C_W is not stable. The carbon atom would move away from the tungsten vacancy site along the c direction, and forms an interstitial defect. Its formation energy is 5.29 eV.

We examine the effect of V_C and V_W imperfections on the electronic properties of tungsten carbide. Fig. 4 shows the valence charge density distribution maps for hexagonal tungsten carbide with a carbon or tungsten vacancy. The electron density in tungsten vacancy is much lower than that in carbon vacancy. This explains the observation of positron annihilation experiments, where the positron lifetime in carbon vacancies is considerably lower than that in W vacancies. Fig. 5 and Fig. 6 present the density of states for tungsten carbide with a carbon and tungsten vacancy, respectively. We use the same supercell and k -grids mesh for the DOS calculation with the defect-free case. Comparison with the DOS of defect-free case (Fig. 1) evinces that carbon and tungsten vacancies induce several peaks in the valley around the Fermi level. In particular, for the DOS of tungsten carbide with a tungsten vacancy, distinct peaks appear about 0.3 eV below Fermi level, and 0.3 and 0.6 eV above EF. While the most notable new feature of DOS for the case of carbon vacancy is a peak centered about 0.2 eV above the Fermi level. Note that, the effects of tungsten vacancy on the electronic properties are more extensive than those of carbon vacancy. Even for this low concentration of vacancies, the presence of the vacancy defects has discernible effects on

the electronic properties of the host crystal.

3.3. Self-interstitial defect

In hexagonal tungsten carbide, there are ten different self-interstitial sites. They are shown in Fig. 7. In naming the self-interstitial sites, we have adopted a similar notation system to those used in pure metal with *hcp* structure[30]. O is the octahedral interstitial sites formed by equivalent three tungsten atoms and three carbon atoms. BOC and BOW are carbon and tungsten basal plane projection of O site, respectively. There exit two different tetrahedral interstitial sites, i.e., TC and TW, which are formed by two different atomic clusters: the former is composed of three carbon atoms and one tungsten atom and the later consists of three tungsten atoms and one carbon atom. Similarly, BTC and BTW are two different hexahedral sites formed by two different atomic clusters: the former is formed by three carbon atoms and two tungsten atoms, while the later is made up of three tungsten atoms and two carbon atoms. C is midway between the nearest-neighbor tungsten atom and carbon atom. BCC/BCW is midway between two nearest carbon/tungsten atoms in the dense \mathbf{a} direction in carbon/tungsten basal plane.

The configurations with carbon or tungsten atom in these interstitial sites are relaxed using the DFT method, and the formation energies of stable configurations are calculated using Eq. (1). In addition, we also give the defect volume changes relative to perfect tungsten carbide using Eq. (2). All results are summarized in Table 4. For interstitial carbon atom, there are four stable or metastable occupation sites, i.e., BOC, BTW, BOW, and BTC. The formation energies of them are 3.41eV, 4.34eV, 5.00eV, and 5.67eV, re-

spectively. The BOC site is the energetically most favorable for interstitial carbon atom, and others are metastable occupation sites. This may be related to the smallest volume change, about 0.75%, induced by the interstitial carbon atom located in BOC site. For interstitial tungsten atom, the formation energies of all interstitial defect configurations are considerably higher. The preferentially occupation site is BOC for interstitial tungsten atom, and the formation energy is 11.51eV. Moreover, there are two complex-defects, namely $I_C(\text{BOC})+W_C$ and $I_C(\text{BTW})+W_C$ (Fig. 9 (b) and (d)), consisting of an interstitial carbon defect and a W_C antisite defect, and which have a little lower formation energy than interstitial tungsten defects. We also observed two crowdion defects along the \mathbf{a} and \mathbf{c} direction, respectively. The formation energies of them are considerably high, about 13.65 and 15.62eV, respectively. Hence, they are energetically highly unfavorable and can not stable in hexagonal tungsten carbide. Comparing to the case of carbon interstitial defects, the defect volume changes of tungsten interstitial defects are much larger.

To sum up, the formation energy of isolated tungsten defects are much larger than that of isolated carbon defects. Antisites and interstitials tungsten defects are clearly energetically less favorable. The key to understanding this large difference lies in the covalent property of W-C bond and the large mismatch in the covalent radii of tungsten ($r_W=1.30\text{\AA}$) and carbon ($r_C=0.77\text{\AA}$). We investigate the consequences of this mismatch on defect formation energies for the example of the tungsten antisite defect (Table 2). By replacing a carbon atom with a tungsten atom the W-C bonds are replaced by W-W bonds. Without atomic relaxation the W-W bonds are 18.4%

too small compared to tungsten bulk. If atomic relaxation is allowed, the six neighboring tungsten atoms move outward by about 0.22\AA . The atomic relaxation is accompanied by an energy gain. However, even large energy gain due to relaxation can not avoid that the tungsten antisite remains energetically unfavorable. The large energy gain is only a response to the huge internal strain which is built up by forming this antisite. Atomic relaxation can reduce this strain; however, it can not completely avoid it.

We also investigate the split-interstitial configuration in hexagonal tungsten carbide. Fig. 8 shows four possible carbon split-interstitial configurations, which are denoted by the symbols SCC, SWC, BSCC, and BSWC, and described as follows: SCC (Fig. 8 (a)), two carbon atoms are symmetrically split in the \mathbf{c} direction about a carbon vacant normal lattice site; SWC (Fig. 8 (b)), a tungsten atom shares a tungsten vacant normal lattice site with a carbon atom in the \mathbf{c} direction; BSCC (Fig. 8 (c)), two carbon atoms are symmetrically split in the dense \mathbf{a} direction about a carbon vacant normal lattice site; BSWC (Fig. 8 (d)), a tungsten atom shares a tungsten vacant normal lattice site with a carbon atom in the dense \mathbf{a} direction. Similar configurations exist for tungsten split interstitials, and are named by SCW, SWW, BSCW, and BSWC, respectively. Note that, the pairs of atoms are approximately $0.5 c_0$ and $2/3 a_0$ apart in the split-interstitial configuration along the \mathbf{c} and dense \mathbf{a} direction, respectively.

Table 5 lists all calculated results of split-interstitial configurations. For the carbon split-interstitial configurations, starting from SCC or BSCC, the relaxations lead to form C-C dimer configurations. Their bond lengths are 1.292 and 1.307\AA , respectively. The formation energies for these two

dimer configurations are 3.53 and 3.14 eV respectively, which are a little higher/lower than that of most stable isolated carbon interstitial defect. It should be pointed out that the dimer centre of BSCC final configuration has shift away the carbon vacant site, as shown in Fig. 9. For tungsten split-interstitial defects, the W-W dimer configuration is not observed. It should be noted that the tungsten will occupy the vacant site when a tungsten atom and a carbon atom share a vacant site.

3.4. Diffusion properties

During isochronal annealing, the defects anneal out in two stages at 800 K and at 1200 K [14]. The 800K stage is attributed by the annealing out of carbon vacancies presumably by long-range migration. Here, we studied the carbon vacancy and interstitial diffusion property in tungsten carbide. In the hexagonal tungsten carbide, there are distinct sites aligned along the \mathbf{c} axis of the materials and in the basal plane. Hence, we investigated two possible transition paths for carbon defects: one path propagates parallel to the \mathbf{c} axis and the other path is the diffusion of carbon defect in the basal plane. The former are denoted as PC_V and PC_I for carbon vacancy and interstitial, respectively; the latter are marked by PB_V and PB_I for carbon vacancy and interstitial. Schematic representations of these diffusion paths are shown in Fig. 10.

For carbon vacancy, the saddle-point structure of PC_V is that the carbon atom equidistant from the two carbon lattice vacant site in the \mathbf{c} direction, i.e. BTW interstitial site (Fig. 10 (a)), while that of PB_V is that the carbon atom seated in the BOC as shown in Fig. 10 (c). The energy barrier of PC_V and PB_V are 6.59 and 3.28 eV, respectively. This very high barrier

indicates that carbon vacancies stay more or less idle for a wide range of temperatures, and possible redistribution or reordering of carbon vacancies requires annealing at very high temperatures. This result provides evidence for the presumption that the 800K stage is attributed by the annealing out of carbon vacancies by long-range migration. It should be pointed out that the former are much higher than the later. This shows that vacancy prefer to diffusion in the basal plane. For the interstitial case, the saddle-point structure of PC_I (Fig. 10(b)) places the interstitial carbon atom in the BOW interstitial sites between its initial and final stable BOC sites, and that of PB_I is a dimer configuration as shown in Fig. 10(d). The energy barriers are 2.20 and 0.36 eV respectively. This lower activation energy evinces that carbon interstitial migration is activated at lower temperatures. As same as the carbon vacancy, interstitial carbon atom preferably diffuse in the basal plane. In addition, the feature of high vacancy diffusion barriers is very important for the stability of carbides, especially in the substoichiometric (WC_x with $x < 1$) case. It implies that once substoichiometric WC are formed, the lattice stays intact because vacancies do not hop to other sites, unless the system are annealed at very high temperatures and for long periods of time. In contrast, carbon interstitial is significantly more mobile for overstoichiometric (WC_x with $x > 1$) case. It means that the structure of overstoichiometric WC are not stable. Our results may give an explanation for that the overstoichiometric phase is not observed in the phase diagram of the W-C system [31].

4. Conclusion

We use first-principles calculations to study the stability of point defects and their complexes in tungsten carbide. Our calculation results confirm that the formation energies of carbon defects are much lower than that of tungsten defects. The outward relaxations around vacancy are found. We identified that the BOC site is the energetically most favorable for interstitial carbon and tungsten atom. The C-C dimer configurations, along c and a direction respectively, are also found and their formation energy are a little higher/lower than that of most stable isolated carbon interstitial defect. In addition, we firstly investigated the atomic-scale mechanism of carbon defect diffusion in tungsten carbide. Isolated carbon defect preferably diffuse in the basal plane. The results of carbon defect diffusion show that the carbon vacancy stay for a wide range of temperature because of extremely high diffusion barriers, while carbon interstitial migration is activated at lower temperatures for its considerable lower activation energy.

Acknowledgement

References

- [1] M. Kaufmann, R. Neu, Fus. Eng. Des. 82 (2007) 521.
- [2] J. Pamela, G.F. Matthews, V. Philipps, R. Kamendje, J. Nucl. Mater. 363C365 (2007) 1.
- [3] R.P. Doerner, J. Nucl. Mater. 363C365 (2007) 32.
- [4] W. Eckstein, J. Roth, Nucl. Instrum. Meth. B 53 (1991) 279.

- [5] H. Kimura, Y. Nishikawa, T. Nakahata, M. Oyaidzu, Y. Oyab, K. Okunoa, *Fus. Eng. Des.* 81 (2006) 295.
- [6] K. Sugiyama, K. Krieger, C.P. Lungu, J. Roth, *J. Nucl. Mater.* 390C391 (2009) 659.
- [7] K.A. Beadle, R. Gupta, A. Mathew, J.G. Chen, B. G. Willis, *Thin Solid Films* 516 (2008) 3847.
- [8] H.W. Hugosson, H. Engqvist, *Int. J. Ref. Met. Hard Mater.* 21 (2003) 55.
- [9] E.I. Isaev, S.I. Simak, I.A. Abrikosov, R. Ahuja, Yu.Kh. Vekilov, M.I. Katsnelson, A.I. Lichtenstein, B. Johansson, *J. Appl. Phys.* 101 (2007) 123519.
- [10] L.F. Mattheiss, D.R. Hamann, *Phys. Rev. B* 30 (1984) 1731.
- [11] A.Y. Liu, R. M. Wentzcovitch, M.L. Cohen, *Phys. Rev. B* 38 (1988) 9483.
- [12] D.L. Price, B.R. Cooper, *Phys. Rev. B* 39 (1989) 4945.
- [13] D.V. Suetin, I.R. Shein, A.L. Ivanovskii, *J. Phys. Chem. Solid* 70 (2009) 64.
- [14] A.A. Rempel, R. Wurschum, and H.E. Schaefer, *Phys. Rev. B* 61 (9),(2000) 5945.
- [15] A.L. Ivanovskii, N.I. Medvedeva, *Mendeleev Commun.* 1 (2001)10.
- [16] N.I. Medvedeva, A.L. Ivanovskii, *Phys. Solid State* 43(2001) 469.

- [17] N. Juslin, P. Erhart, P. Träkelin, J. Nord, K.O.E. Henriksson, K. Nordlund, E. Salonen, and K. Albe, *J. Appl. Phys.* 98 (2005) 123520.
- [18] C. Bjökas, K. Vötler, and K. Nordlund, *Phys. Rev. B* 74 (2006) 140103.
- [19] G. Kresse and J. Hafner, *Phys. Rev. B* 47 (1993) 558.
- [20] G. Kresse and J. Furthmüller, *Phys. Rev. B* 54 (1996) 11169.
- [21] G. Kresse and D. Joubert, *Phys. Rev. B* 59 (1999) 1758.
- [22] P.E. Blöchl, *Phys. Rev. B* 50 (1994) 17953.
- [23] J.P. Perdew, J.A. Chevary, S.H. Vosko, K.A. Jackson, M.R. Pederson, D.J. Singh, and C. Fiolhais, *Phys. Rev. B* 46 (1992) 6671; 48 (1993) 4978(E).
- [24] H.J. Monkhorst, J.D. Pack, *Phys. Rev. B* 13 (1976) 5188.
- [25] H.O. Pierson, *Handbook of Refractory Carbides and Nitrides: Properties Characteristics, Processing, and Applications* Noyes, Westwood, NJ, 1996.
- [26] H.L Brown, P.E. Armstrong, C.P. Kempter, *J. Chem. Phys.* 45 (1966) 547.
- [27] *CRC Handbook of Chemistry and Physics*, 85th ed., edited by D. R. Lide(CRC, Boca Raton, 2004).
- [28] N. Gaston, S. Hendy, *Catalysis Today* 146 (2009) 223.
- [29] L. Tsetseris, S.T. Pantelides, *Acta Materialia* 56 (2008) 2864.

[30] F. Willaime, *J. Nucl. Mater.* 323 (2003) 205.

[31] A.S Kurlov, A.I Gusev, *Russian Chemical Reviews* 75(7) (2006) 617.

Table 1 The bulk properties and cohesive energy (E_c) of tungsten carbide, MD and DFT mean the results obtained by molecular dynamic simulation and density functional theory, respectively.

	a_0	c_0/a_0	$B_0(\text{Mbar})$	$E_c(\text{eV})$
Experiment	2.907 ^a	0.976 ^a	3.29 ^b	-16.68 ^c
MD ^d	2.917	0.964	4.43	-16.68
DFT ^d	2.979	0.975	3.68	-15.01
Present work	2.932	0.973	3.56	-16.42

^a Reference [25]

^b Reference [26]

^c Reference [27]

^d Reference [17]

Table 2 $D(R)(\text{\AA})$ is the distance between neighbor atom R ($R=W_{Vc}^N, C_{Vc}^c, C_{Vc}^b$) and defect lattice site; $\Delta V/V$ (%) is defect volume changes relative to the perfect system; E_f (eV) is the formation energy of defect in

	configuration.		
	Perfect	V_C	W_C
$D(W_{Vc}^N)$	2.214	2.231	2.454
$D(C_{Vc}^c)$	2.854	2.842	2.817
$D(C_{Vc}^b)$	2.932	2.908	3.023
$\Delta V/V$		-0.2	3.4
E_f		0.39	8.69

Table 3 $D(R)(\text{\AA})$ is the distance between neighbor atom R ($R=C_{Vw}^N$, W_{Vc}^c , W_{Vc}^b) and defect lattice site; $\Delta V/V$ (%) is defect volume changes relative to the perfect system; E_f (eV) is the formation energy of configuration.

	Perfect	V_W	C_W
$D(C_{Vw}^N)$	2.214	2.311	2.330
$D(W_{Vc}^c)$	2.854	2.762	2.809
$D(W_{Vc}^b)$	2.932	2.900	2.911
$\Delta V/V$		-0.4	-0.1
E_f		4.14	8.81

Table 4 Calculation results for carbon and tungsten self-interstitial defects in tungsten carbide. $\Delta V/V$ (%) is defect volume changes relative to the perfect system; E_f (eV) is the formation energy of defect configuration.

	Carbon interstitial defect			Tungsten interstitial defect		
	Final configuration	E_f	$\Delta V/V$	Final configuration	E_f	$\Delta V/V$
O	BOC	3.41	0.75	BOC	11.58	4.67
BOC	BOC	3.41	0.75	BOC	11.58	4.67
BOW	BOW	5.00	1.82	BOW	13.48	4.94
C	BOC	3.41	0.75	$I_C(\text{BOC})+W_C$	9.73	3.80
BCC	BOC	3.41	0.75	BOC	11.58	4.67
BCW	BTW	4.37	1.96	c -Crowdion	13.65	5.32
TC	BTC	5.63	1.74	a -Crowdion	15.62	5.00
BTC	BTC	5.63	1.74	a -Crowdion	15.62	5.00
TW	BTW	4.37	1.96	$I_C(\text{BTW})+W_C$	10.65	5.21
BTW	BTW	4.37	1.96	BTW	15.96	5.94

Table 5. Formation energy of final defect configurations obtained from the relaxation of split interstitial configurations. $\Delta V/V$ (%) is defect volume changes relative to the perfect system; E_f (eV) is the formation energy of defect configuration.

	Final configuration	E_f	$\Delta V/V$
SCC	<i>c</i> -Dimer	3.53	2.08
SWC	I_C (BTC)	5.63	1.74
BSCC	<i>a</i> -Dimer	3.14	1.64
BSWC	I_C (BTW)	4.37	1.96
SCW	I_C (BTW)+ W_C	10.69	5.21
SWW	<i>c</i> -Crowdion	15.62	5.00
BSCW	I_C (BOC)+ W_C	9.73	3.80
BSWW	<i>a</i> -Crowdion	13.76	5.32

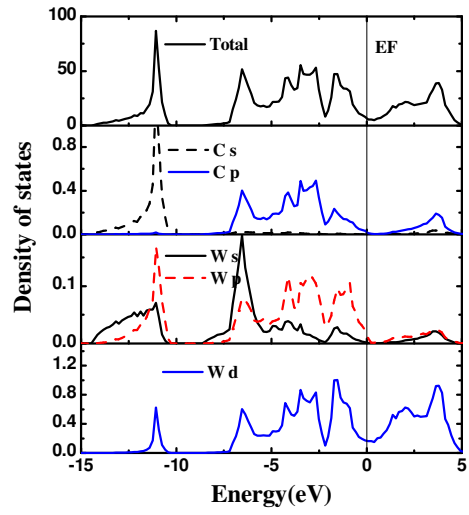


Figure 1: (color online) The total and partial contributions to the DOS from orbital of different angular symmetry on carbon and tungsten site of hexagonal tungsten carbide. Zero of energy is set at the Fermi level.

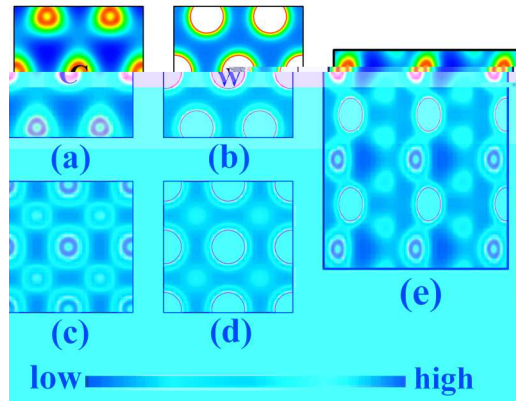


Figure 2: (color online) The valence charge density distribution maps for hexagonal tungsten carbide: (a) and (b) show the valence charge density distribution for the carbon and tungsten basal plane, respectively; (c) and (d) present the valence charge density distribution for carbon and tungsten (1 0 -1 0) plane, respectively; (e) are the valence charge density in (1 1 -2 0) plane.

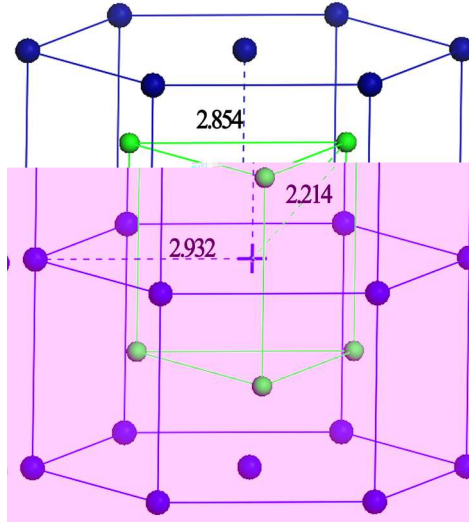


Figure 3: (color online) The local structure of hexagonal tungsten carbide with a carbon vacancy. The tungsten and carbon atoms are marked in green (white) and blue (black) balls, respectively. The "+" denotes the carbon vacant site. The dash line is the distance between carbon vacant and its neighbors: 2.214Å, 2.854Å and 2.932Å.

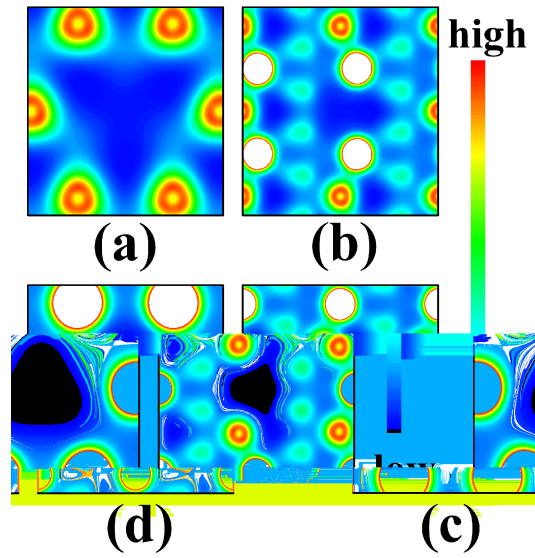


Figure 4: (color online) The valence charge density distribution maps for hexagonal tungsten carbide with vacancy defect: (a) and (b) are the valence charge density of WC with carbon vacancy in the carbon basal plane and the $(1\ 1\ -2\ 0)$ plane, respectively; (c) and (d) are the valence charge density of WC with tungsten vacancy in the tungsten basal plane and the $(1\ 1\ -2\ 0)$ plane, respectively.

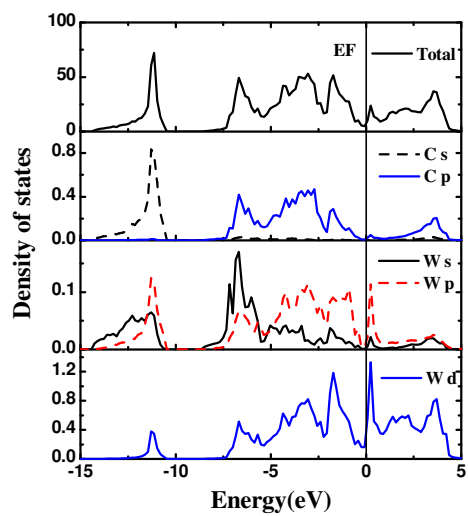


Figure 5: (color online) Density of states for tungsten carbide with a carbon vacancy.

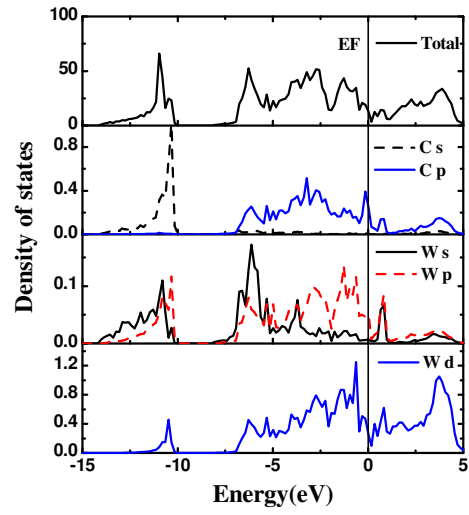


Figure 6: (color online) Density of states for tungsten carbide with a tungsten vacancy.

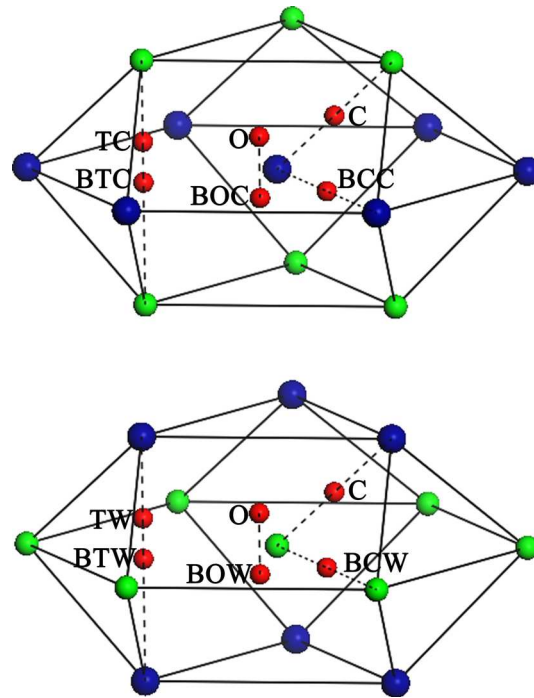


Figure 7: (color online) Schematic diagram of various isolated interstitial sites in tungsten carbide. The tungsten and carbon atoms are marked in green (white) and blue (black) balls, respectively. The smaller red (dark gray) balls represent the interstitial sites.

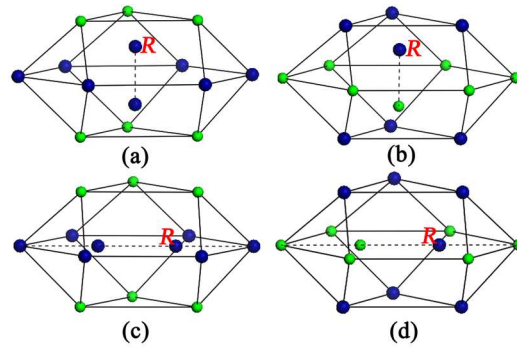


Figure 8: (color online) Schematic diagram of four carbon split-interstitial configurations in tungsten carbide. The tungsten and carbon atoms are marked in green (white) and blue (black) balls, respectively. For tungsten split-interstitial configurations, the carbon atom denoted by red R would be replaced by tungsten atom.

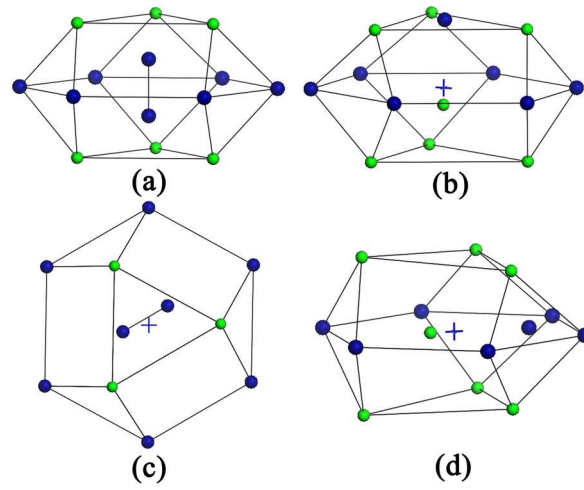


Figure 9: (color online) Schematic diagram of final configurations in tungsten carbide with a interstitial carbon or tungsten atom. The tungsten and carbon atoms are marked in green (white) and blue (black) balls, respectively. The "+" denotes the carbon vacant site.

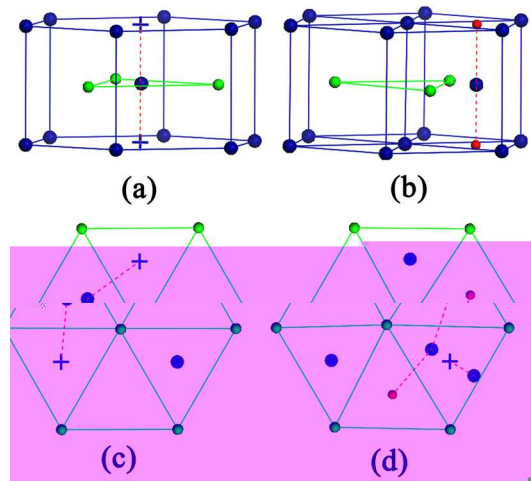


Figure 10: (color online) Schematic of the mechanism for carbon vacancy and interstitial in tungsten carbide: (a) and (b) show diffusion paths PC_V and PC_I , respectively, while (c) and (d) are diffusion paths PB_V and PB_I , respectively. The "+" denoted the initial and final vacancy site, and the small red balls are the initial and final interstitial sites BOC. The red dash lines are guides to the eyes for these diffusion paths. The blue and green balls are the tungsten and carbon atoms, respectively, in the saddle-point structure. The tungsten and carbon atoms are marked in green (white) and blue (black) balls.